

Technical Report

Round robin test on angle of repose: DEM simulation results collected from 16 groups around the world

Hidetaka Saomoto^{a,*}, Naotaka Kikkawa^b, Shuji Moriguchi^c, Yukio Nakata^d, Masahide Otsubo^{e,1}, Vasileios Angelidakis^{f,2}, Yi Pik Cheng^g, Kevin Chew^h, Gabriele Chiaro^h, Jérôme Duriezⁱ, Sacha Duvergerⁱ, Joaquín Irazábal González^j, Mingjing Jiang^{k,3}, Yohei Karasaki^e, Akiko Kono^l, Xintong Li^m, Zhuyuan Linⁿ, Asen Liu^m, Sadegh Nadimi^f, Hitoshi Nakase^o, Daisuke Nishiura^p, Utsa Rashique^q, Hiroyuki Shimizu^r, Kumpei Tsuji^s, Takashi Watanabe^t, Xiaomin Xu^u, Mourad Zeghal^q

^a Institute of Earthquake and Volcano Geology, National Institute of Advanced Industrial Science and Technology, Ibaraki, Japan

^b Construction Safety Research Group, National Institute of Occupational Safety and Health, Japan, Tokyo, Japan

^c International Research Institute of Disaster Science, Tohoku University, Miyagi, Japan

^d Graduate School of Sciences and Technology for Innovation, Yamaguchi University, Yamaguchi, Japan

^e Institute of Industrial Science, The University of Tokyo, Tokyo, Japan

^f School of Engineering, Newcastle University, Newcastle upon Tyne, United Kingdom

^g Department of Civil, Environmental and Geomatic Engineering, University College London, London, United Kingdom

^h Civil and Natural Resources Engineering, University of Canterbury, Christchurch, New Zealand

ⁱ RECOVER, INRAE, Aix Marseille University, Aix-en-Provence, France

^j Machine Learning in Civil Engineering Group, International Centre for Numerical Methods in Engineering (CIMNE), Barcelona, Spain

^k School of Civil Engineering, Suzhou University of Science and Technology, Jiangsu Province, China

^l Railway Dynamics Division, Railway Technical Research Institute, Tokyo, Japan

^m School of Civil Engineering, Tianjin University, Tianjin, China

ⁿ Department of Earth Science and Engineering, Nanjing University, Jiangsu, China

^o Research And Business Incubation Unit, Tokyo Electric Power Services Co., Ltd., Tokyo, Japan

^p Center for Mathematical Science and Advanced Technology, Japan Agency for Marine-Earth Science and Technology, Kanagawa, Japan

^q Civil and Environmental Engineering, Rensselaer Polytechnic Institute, New York, United States

^r Civil Engineering Design Division, Kajima corporation, Tokyo, Japan

^s Department of Civil Engineering, Kyushu University, Fukuoka, Japan

^t Disaster Reduction and Environmental Engineering Dept., Kozo Keikaku Engineering Inc., Tokyo, Japan

^u Department of Engineering, Civil Engineering Division, University of Cambridge, Cambridge, United Kingdom

Received 4 July 2022; received in revised form 1 December 2022; accepted 14 December 2022

Abstract

The round robin test (the simultaneous analysis of the same problem) is a method to investigate the variance and sensitivity of results provided by different analysts for a given problem and the reliability of the particular software used by each group participating in the test. A round robin test has been conducted for the traditional numerical method (e.g., finite difference method), but not yet for the discrete element method (DEM). This paper presents the results of the first ever round robin test on the DEM simulation for the angle of

* Corresponding author.

E-mail address: h-saomoto@aist.go.jp (H. Saomoto).

¹ Present affiliation: Public Works Research Institute, Ibaraki, Japan.

² Present affiliation: Friedrich-Alexander-Universität Erlangen-Nürnberg, Erlangen, Germany.

³ Former affiliation: Tianjin University, Tianjin, China.

repose, involving 16 groups from around the world using different softwares. Within the scope of this round robin test, most groups reported similar simulation results for the angle of repose that differed only by a few degrees from the average of the experimental values, which was initially concealed from participants. There was also good agreement on the degree of variance of the angle of repose. In addition, this paper revealed the recent trends on the interparticle constitutive models and DEM softwares by considering the reports obtained from the participants.

© 2023 Production and hosting by Elsevier B.V. on behalf of The Japanese Geotechnical Society. This is an open access article under the CC BY-NC-ND license (<http://creativecommons.org/licenses/by-nc-nd/4.0/>).

Keywords: Round robin test; Discrete element method; Angle of repose; Validation; Particle; 3D printer

1. Introduction

The discrete element method (DEM) was developed in the 1970s (Cundall, 1971; Cundall and Strack, 1979) and has now become a powerful tool for analyzing the complex behavior of geomaterials featuring particulate assemblies subjected to large deformation and fracturing.

One of the most popular applications of DEM in soil mechanics is to simulate soil element tests, such as the triaxial compression test and the direct shear test. One of the important purposes of simulating soil element tests by DEM is to calibrate the parameters of the interparticle constitutive model by fitting the stress–strain curve obtained from the element tests. After parameter adjustment, the relationship between the microstructure properties, such as particle arrangement, to the macroscopic stress–strain relationship can be discussed. Cheng et al. (2003) created particles that can represent particle fragmentation by bonding about 40 spheres together. They simulated a triaxial compression test using about 400 of these crushable particles. Kikkawa et al. (2013) measured elastic wave velocities of chemical-solidified Toyoura sand using a bender element test and then used the test results to determine the elastic stiffness of contacting DEM particles and the bond stiffness bridging DEM particles. Jiang et al. (2015) proposed an interparticle constitutive model that can account for the rolling and twisting between non-spherical particles and conducted triaxial compression simulations incorporating the proposed model using spherical particles. In their simulation model for triaxial compression tests which included methane hydrate particles, Yu et al. (2016) simulated the stress–strain curve by changing the content of methane hydrate particles inside the simulation model. Otsubo and O’Sullivan (2018) conducted elastic wave propagation tests using particles made of borosilicate glass with controlled surface roughness. These were simulated by a DEM that incorporates an interparticle constitutive model considering surface roughness (Otsubo et al., 2017) and discussed the effect of the particle surface roughness on the macroscopic shear stiffness. Chew et al. (2022) conducted DEM simulations for direct shear tests of gravel-rubber mixtures. The gravel and rubber particles were respectively modeled using clamped particles of five different shapes.

In addition to the soil element test, the DEM simulations coupled with fluids have been actively studied. Zeghal and El

Shamy (2004) simulated liquefaction by coupling DEM with the Navier–Stokes (NS) equations averaged through porosity. Yamaguchi et al. (2017) modeled a channel bed with a DEM and simulated the topographic changes in the channel bed caused by water flowing in the channel. Tsuji et al. (2019) attempted to simulate the ground collapse due to the deterioration of sewer pipes using the DEM and the smoothed particle hydrodynamics (SPH) representing the pore fluid phase. Chen et al. (2022) applied a large-scale DEM simulation code (DEPTH) to the underwater mixing process for deep-sea mining with lubrication models.

The DEM is applied in engineering to simulate the ballast behavior under rails caused by railroad loads. Because ballast particles are about 5 cm in diameter, a simulation model close to the actual condition can be created by using a high-performance computer. For example, Irazábal et al. (2017) determined the parameters of a bounded rolling friction model to simulate ballast particles with spherical particles through a comparison with experimental results. Kono (2018) modeled the accurate ballast shape by combining the laser measurement and a shape optimization method for clumping proposed by Matsushima and Saomoto (2002). The ballast particles were then subjected to DEM analysis and compared with the results of cyclic loading tests. In their analysis of the behaviors of 190,000 ballast particles, Nishiura et al. (2018) used the quadruple discrete element method (QDEM) in which the material parameters are directly determined from the macroscopic viscoelastic parameters used in continuum mechanics. In addition to determining ballast behavior, there are other engineering-oriented applications of DEM simulations: slope hazards (Nakase et al., 2017); rockfall protection (Kanno et al., 2021); rock engineering (Duriez et al., 2011; Shimizu et al., 2011; Jiang et al., 2020); and clay deformation (Lin et al., 2021).

The DEM simulations in almost all of the DEM applications described above have been validated by a single analysis group using a single software. From this perspective, it is difficult to evaluate the skill of each analyst and to determine the reliability of the software by referring to these studies individually. This brings us to the motivation of our study.

Round robin test for traditional numerical methods such as the finite element method have been conducted over the years for different research fields: seismology (Harris et al., 2011; Harris et al., 2018); rock mechanics

(Berre et al., 2021); coastal hydrology (Horrillo et al., 2015). These round robin tests indicate that assessing the user-dependency and sensitivity of results and the reliability of each software is extremely important. It should be noted that despite the importance of the round robin test, it has never been implemented for a DEM simulation.

We therefore have conducted the first ever round robin test on DEM simulation for the angle of repose (AOR) under the responsibility of the TC105 Japanese domestic committee in the Japanese Geotechnical Society. The objectives of this study are as follows: (1) To clarify the approach taken by the participants of the round robin test to the simulation of the angle of repose; (2) To quantitatively analyze the differences between individual simulation results and experimental results, based on both the average value and the variance; (3) To discuss the relationship between the differences from experiments and the modeling techniques especially for particle shape modeling and inter-particle constitutive equation; and (4) To clearly see the current trend in the DEM software.

2. Round robin test for discrete element method

Although the details of the round robin test are found on the website (TC105 Japanese domestic committee, 2020) and Nakata et al. (2022), we summarize and describe that information here for the convenience of the readers.

2.1. Outline of round robin test

Figure 1 shows the outline of the round robin test for the AOR. Using the artificial particles detailed in Section 2.2, the TC105 Japanese committee (test organizer) conducted two types of experiments for the AOR depicted in Section 2.3. After obtaining the experimental results, the committee released the information relating to the particles used in the experiments (material, shape, mechanical properties) and the two experimental conditions required for the DEM simulation to the participating groups via the website (TC105 Japanese domestic committee, 2020). These groups then performed DEM simulations for the experimental conditions based on their research experiences and perspectives using the information available on the website and then submitted the simulation results to the committee in accordance with the report format described in Section 2.5.

2.2. Artificial particle used in experiments

Figure 2 shows the shape of the artificial particles, used in the experiment. Each artificial particle was designed with four spheres (spheres 1, 2, 3, and 4) placed at each vertex of a regular tetrahedron. Note that there is no size distribution for artificial particles used in the experiments. Subsequently, the artificial particles were realized with resinous

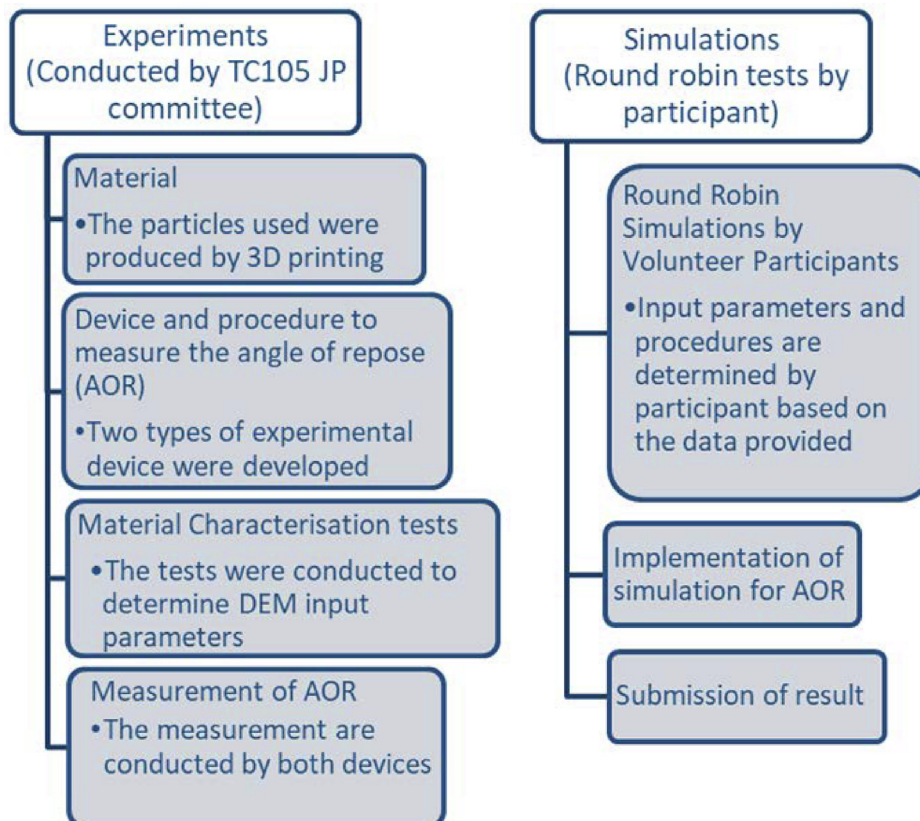


Fig. 1. Outline of the round robin test for AOR.

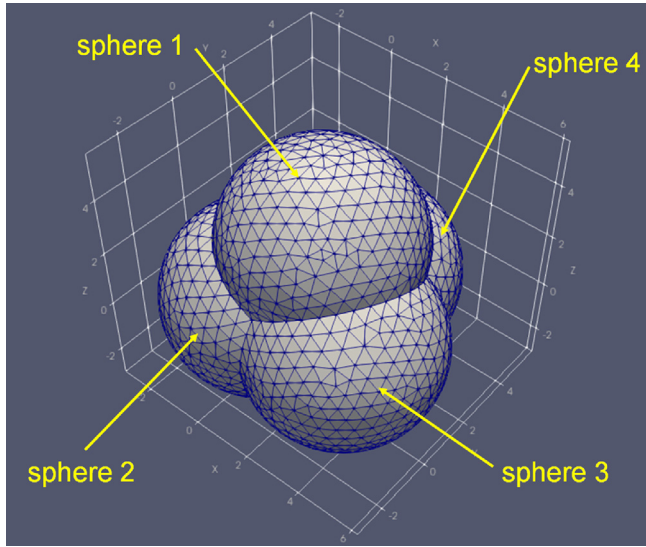


Fig. 2. Shape of artificial particles represented by four spheres arranged in a regular tetrahedral form.

material by using a 3D printer. The coordinates of each sphere center are expressed as follows: (0, 0, 0), (3.101, 0, 0), (1.551, 0.895, 2.532), and (1.551, 2.685, 0) for spheres 1, 2, 3, and 4, respectively (unit: mm). Note that each sphere has the same radius (3.101 mm).

The material properties of the artificial particles are listed in Table 1. The mean values and standard deviations of each parameter were obtained by a sufficient number of experiments. In addition to the information listed in Table 1, friction angles between the artificial particle material (resin) and the surface of the experimental apparatus (acrylic plate) have also been measured (Nakata et al., 2022): static friction angle: 27.2 degrees with the standard deviation of 4.26 degrees; dynamic friction angle: 16.5 degrees with the standard deviation of 7.35 degrees.

2.3. Two types of AOR experiment

The test organizer prepared two types of AOR experimental setup: Device I is a rectangular type (plane strain

condition), as shown in Fig. 3, and Device II is a cylindrical type (axial-symmetric condition), as shown in Fig. 4.

The Device I apparatus is made of transparent acrylic plates and comprises an upper and a lower box, separated by a horizontal acrylic plate that can translate horizontally. The artificial particles (detailed in Section 2.2) are initially deposited in the upper acrylic box. During the experiment, the artificial particles firstly fall under the action of gravity by translating the plate installed between the upper box and the lower box outwards. When the particles have come to rest, the front panel of the lower box is pulled upwards by an electric motor at a constant speed of 43 mm/s. Almost 2500 particles were used in those experiment. We can also confirm the size detail on the website (TC105 Japanese domestic committee, 2020).

A schematic illustration of Device II with the cylindrical configuration is provided in Fig. 4. The container in which the particles are placed [a] is enclosed by an acrylic cylindrical wall [d] and a fixed bottom plate [e] with a diameter of 160 mm. The cylindrical wall can be moved down at a constant speed using an electric motor [b], and the initial height from the top of the cylindrical wall to the bottom plate is 90 mm. Two digital cameras [h] are placed orthogonally in order to measure the angle of repose. The experimental procedure for Device II is as follows: (1) the artificial particles are initially deposited in a hopper of 100 mm diameter; (2) the container [a] is filled with 2468 particles under the action of gravity by translating the bottom plate of the hopper.

The aforementioned experimental procedure was described in detail on the website (TC105 Japanese domestic committee, 2020) prior to the round robin test. Therefore, the participants were expected to perform DEM simulations according to the experimental process for each device.

2.4. AOR measurement in experiment

Figure 5 shows a schematic illustration at the end of the DEM simulation for Device I. The AOR for Device I is uniquely determined using the coordinate values of the cen-

Table 1
List of characteristics of the artificial particles.

Parameter	Test	Object	Mean	Standard deviation
Static friction angle	Inclined surface test	Resin-resin	35.5°	3.82°
		Acrylic-resin	27.2°	4.26°
Dynamic friction angle	Inclined surface test	Resin-resin	29.36°	2.42°
		Acrylic-resin	16.5°	7.35°
Coefficient of restitution	Drop test	Resin-resin	0.809	0.0115
		Acrylic-resin	0.790	0.0280
Shear modulus	Cyclic uniaxial test	Resin	560 MPa	158 MPa
		for horizontal plane	680 MPa	70 MPa
		for vertical plane	440 MPa	130 MPa
Normal spring coefficient (Normal contact force: 0.1 N)	Cyclic uniaxial test	Resin	6.0×10^4 N/m	1.1×10^4 N/m
		for horizontal plane	6.9×10^4 N/m	0.5×10^4 N/m
		for vertical plane	5.2×10^4 N/m	0.5×10^4 N/m

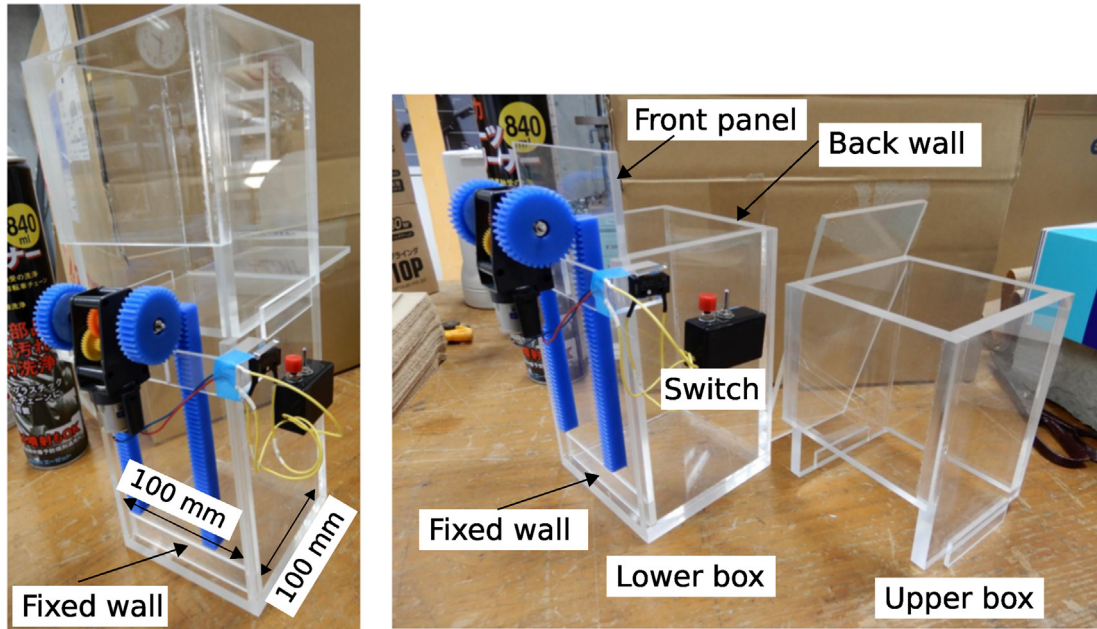


Fig. 3. Experimental apparatus for Device I.

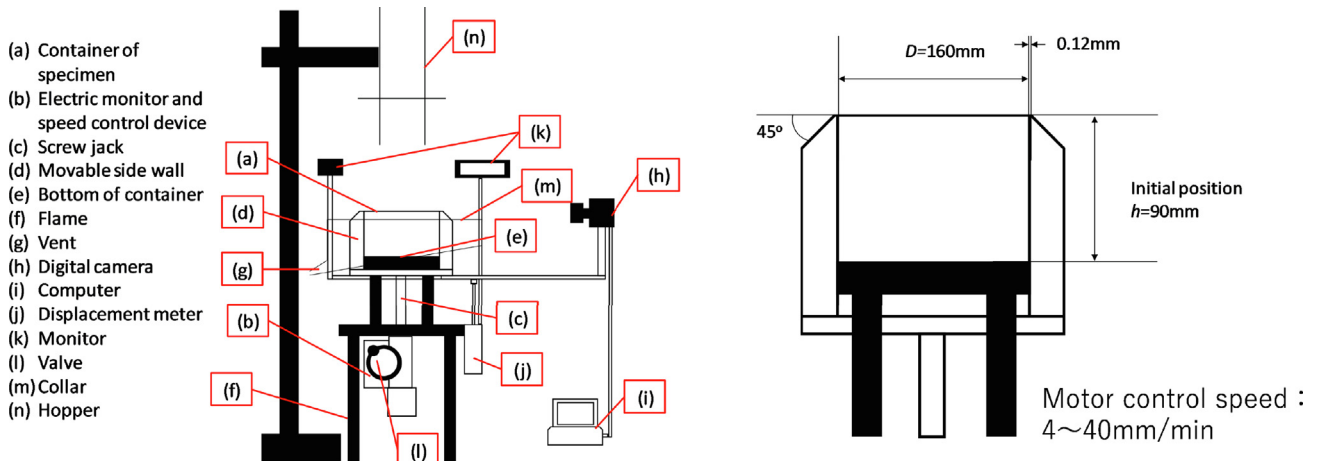


Fig. 4. Experimental apparatus for Device II (left: overall view, right: container section where particles are deposited).

troid of the apex sphere at the top of the specimen (Fig. 5). Using lengths Z and L depicted in Fig. 5, we have

$$\theta_I = \tan^{-1} \left(\frac{Z}{L} \right), \quad (1)$$

where θ_I is the AOR for Device I.

In the case of Device II, we can use the coordinate values of the apex sphere of a particle at the end of simulation to determine the AOR, in the same way as described for Device I. Note that there are several possible definitions of the AOR for Device II.

Figure 6 is a supporting diagram to define the angle of repose in Device II, indicating a schematic illustration at the end of the DEM simulation for Device II. In general, the xy-coordinate of the sphere located at the top (a) does

not coincide with the bottom plate center (O). To this end, 360 measuring points were set on the top of the cylindrical wall at intervals of one degree, and the angle θ_i was calculated for each line connecting each measuring point (i) and the top of the sphere element (a). Denoting the maximum θ_i as θ_{max} and the minimum θ_i as θ_{min} , the average of these two values can be a representative of angle of repose for Device II. Here, we employ this definition as the AOR for Device II,

$$\theta_{II} = \frac{\theta_{max} + \theta_{min}}{2}, \quad (2)$$

where θ_{II} is the the AOR for Device II. Naturally, Eqs. (1) and (2) are applied to the corresponding DEM simulation results in order to quantitatively compare the simulation results and the experimentally obtained results.

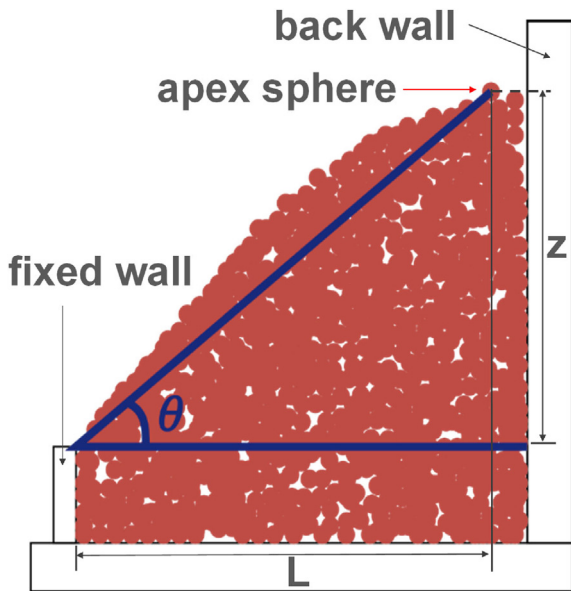


Fig. 5. Schematic illustration at the end of DEM simulation for Device I.

It should be noted that the value of AOR generally depends on the initial configuration of particles and subsequent packing characteristics. However, since it is difficult to analyze such effects quantitatively and independently, we tried to compare the experimental data with simulation results based on the concept that the effect is one of the uncertainties which causes variation of the AOR.

2.5. Data collection from participants

Each participating group is required to submit a spreadsheet containing the predefined questions prepared by the test organizer and the 3D coordinates of all sphere particles included in tetrahedral particles at the end of the simulation. The questions in the spreadsheet are designed to gather specific information, including the following: (1) the software used, (2) the parallel computation environment, (3) the interparticle constitutive model and its parameter values, (4) the particle shape and the size used,

(5) the method of creating the initial configuration of particles, (6) the setting of the moving speed of the boundary wall, and (7) the number of simulation trials.

3. Results of round robin test

This section summarizes the results of the round robin test where the reported AOR values are correlated with the adopted input parameters for each analysis group. It should be noted that the results of the round robin test are not necessarily general but limited to the specific conditions in the experiments, such as boundary conditions, artificially-made particles, and low confining pressure.

3.1. Number of participation groups by country

The number of groups who participated in the round robin test by country is shown in Fig. 7. In total, 16 groups from 7 countries participated in the round robin test. According to Fig. 7, Japan has the largest number of analysis groups, followed by China and the UK, and France, New Zealand, Spain, and the United States are represented by an equal number of groups.

3.2. Summary for used software

The statistical results of the software used in the round robin test are illustrated in Fig. 8. It can be seen that software most commonly used in the round robin test was PFC3D (Itasca Consulting Group Inc, 2021) and in-house software. Yade (Smilauer et al., 2021) was used by two groups. Also, LIGGGHTS (Kloss et al., 2012), LAMMPS (Sandia National Laboratories, 2001; Thompson et al., 2022), HiDEM (Sakaguchi and Nishiura, 2009), DEPTH (Chen et al., 2020, Nishiura et al., 2021), and Kratos Multiphysics (Dadvand et al., 2010; Dadvand et al., 2013) were all used by one group.

A brief introduction to the various software chosen for the assigned task follows. The PFC3D is a prominent commercial software manufactured by ITASCA Consulting

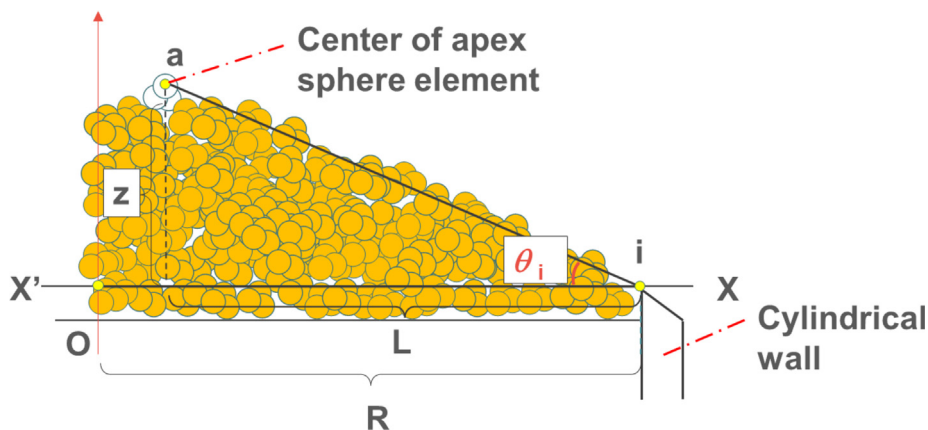


Fig. 6. Schematic illustration at the end of DEM simulation for Device II.

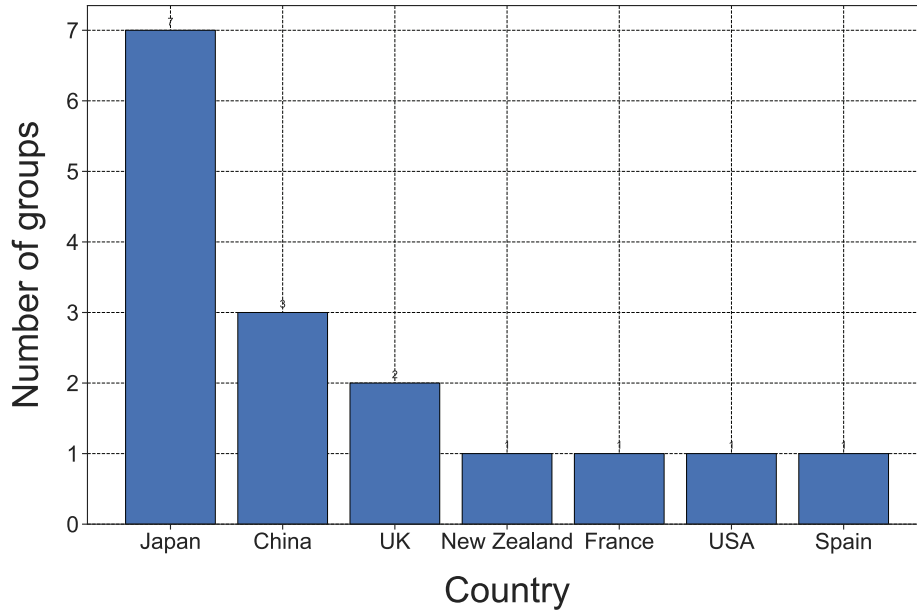


Fig. 7. Relationship between the number of analysis groups and country.

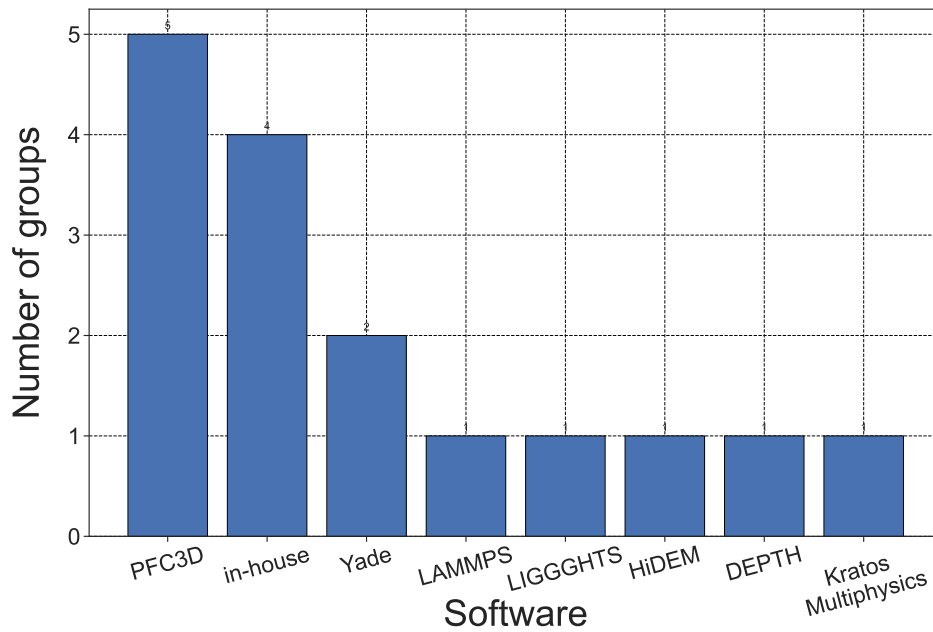


Fig. 8. Histogram of software used in round robin test.

Group, Inc. and is widely used in discrete element simulations in the field of geotechnical engineering.

Most in-house software is developed independently in university laboratories. Note that we did not investigate the details of them used in the round robin test.

Yade is an open-source framework for DEM simulations. Although the core computation parts are written in C++, the user interface is prepared with the Python language for easy handling.

LIGGGHTS is an open-source discrete element simulator and is an extension of the molecular dynamics software, LAMMPS (described below). In comparison with

LAMMPS, LIGGGHTS has the following additional features: CAD geometry handling, heat conduction, contact force formulation, and particle arrangement using 3-D meshes.

LAMMPS is a classical molecular dynamics simulation code (open-source). While LAMMPS is designed for molecular dynamics simulations, it comes with an original granular mechanics package which is to be distinguished from LIGGGHTS.

HiDEM is a Fortran 90/95 based commercial software developed by Japan Agency for Marine-Earth Science and Technology (JAMSTEC). Furthermore, DEPTH is a

commercial software developed from HiDEM that implements an iterative dynamic load balancer algorithms (Furuichi et al., 2017) enabling it to run the world’s largest-scale DEM simulation on the massive parallel computer systems.

KRATOS Multiphysics is an open-source framework for building parallel, multi-disciplinary simulation software including the discrete element method. This software features easy coupling of the DEM with other analysis tools implemented in KRATOS, such as the DEM and a fluid analysis or the DEM and a finite element solid analysis.

3.3. Modeling for particle shape and mass

Figure 9 shows the relationship between the AOR and the density of the clumped particle for both Device I (Fig. 9 (a)) and Device II (Fig. 9 (b)). In Fig. 9, the vertical axis indicates the value of the angle of repose and the horizontal axis indicates the density used in the DEM simulations. The solid red line drawn horizontally represents the mean of the experimental AOR values, and the dashed darkred and blue lines represent the 75% and 97.5% quartiles, respectively. The vertical line with a density close to 10^3 indicates the density of the material of particles used in the experiments (1111 kg/m^3). Each plot shows the AOR calculated from the DEM simulation results submitted by the participants, and the legend indicates the analyst ID (16 groups in total), respectively. Note that the experimental value (1111 kg/m^2) was employed in 91% of the total number of simulation runs for Device I (350 runs in total) and in 87% of the total number of simulation runs for Device II (343 runs in total).

Most of the analysis groups used tetrahedron-shaped particles by clumping four spheres as in the experiment, while the particles used by several other analysis groups had their own user-defined shape or were spherical. When using a spherical particle shape, which differs from the experimental one, it is necessary to adjust the interparticle

constitutive model reflecting the particle shape effect which is equivalent to the experimental state in terms of the rotational motion of the particles and the porosity ratio of the particle assembly. For example, analysis group 14 used spherical particles and introduced the rolling resistance of spherical particles to account for the effect of particle shape. Most analysis groups used the same size particles as those in the experiment.

From the perspective of accuracy, most of the simulation results fell within the 97.5% quantile of the AOR obtained from the experiments (assuming normal distribution) irrespective of the device type. Some simulation results deviated from the experimental values (analysis groups 2 and 4 for Device I, and analysis groups 2, 4, and 7 for Device II), but these are basically due to inappropriate parameter settings, which will be discussed in a later section. In the case of analysis group 6, the AOR recorded from the DEM simulations was smaller than the experimental value, because rounded convex tetrahedral potential particles were employed. These particles interlocked less than the real behavior that was expected for the concave tetrahedral particles. Nevertheless, this modeling approach provided a quantification of the effect that convexity effects on the interlocking capabilities of the analyzed material. There were two cases in which the values of density were significantly different from the experimental values: analysis group 2, with about 300 kg/m^3 and analysis group 4, with $10,000 \text{ kg/m}^3$. The authors guess the analysis group 4 may aim to reduce the computational cost by increasing the time step in the DEM simulation, whereas the intention of group 2 is unclear. The details of the inappropriate settings are described in the following discussion section.

In the case where the density is set to a slightly smaller value (analysis group 6) than the experimental value, it seems that the volume of the user-defined particle shape (rounded tetrahedral potential particle shape) illustrated in Fig. 10 slightly differs from that of the particles used in the experiment, to approximate closely the real

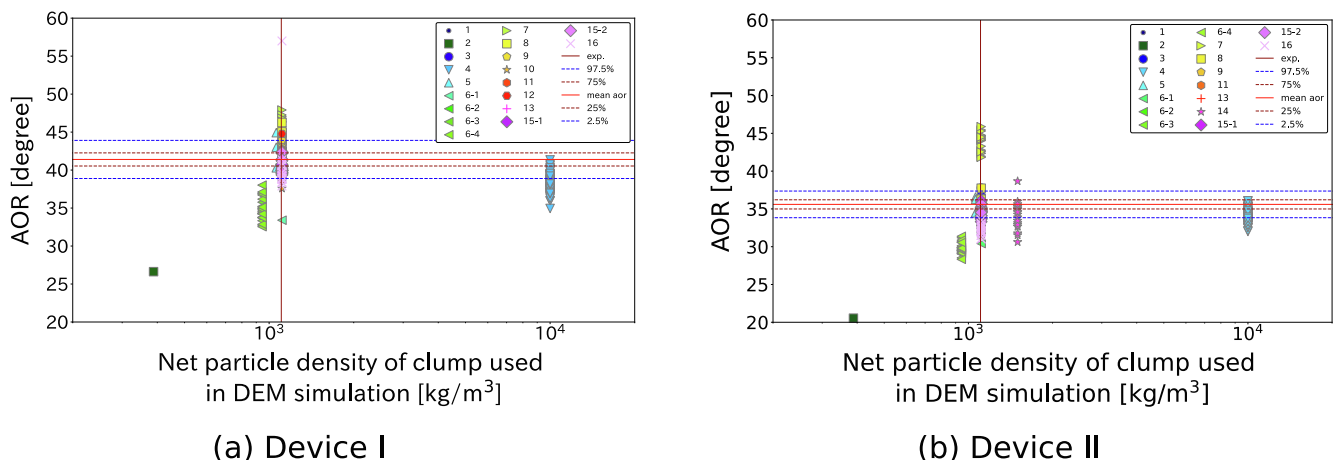


Fig. 9. Relationship between AOR experiment results and net particle density used in DEM simulations.

inertial characteristics (mass and inertia) of the physical particle.

3.4. Summary for interparticle constitutive model and simulation time step

Figure 11 indicates the histogram of the interparticle constitutive model used by the analysis groups. The most-used interparticle constitutive model was the Voigt model, followed by the Hertz-Mindlin model. Most of the groups that used particles with the same shape as the tetrahedral particle used in the experiment adopted the Voigt model or the Hertz-Mindlin model. Meanwhile, the groups that used spherical particles adopted interparticle constitutive models incorporating rotation resistance corresponding to the particle shape effect.

Since all the constitutive equations require normal stiffness, we first check the setting of the normal stiffness. In addition, because normal directional stiffness is related to the time step setting, normal stiffness is an important parameter in this sense.

Figure 12 shows the relationships between the AOR and the normal stiffness for both Device I (Fig. 12 (a)) and Device II (Fig. 12 (b)). The horizontal axis shows the normal stiffness used in the DEM simulations. The meanings of the vertical axis and legend are the same as described in Fig. 9. The normal stiffness for the Hertz-Mindlin contact model varies non-linearly with the applied normal force (F_n) or overlap (δ_n) between two sphere elements in contact. Considering the height of sample ($\simeq 0.1$ m) and the material density (1111 kg/m³), a representative normal force of 0.1 N was used to estimate the secant normal stiffness (K_n) using the following expression:

$$K_n = \frac{F_n}{\delta_n} = \frac{2}{3} (6E^*R^*)^{\frac{1}{3}} F_n^{\frac{1}{3}}, \quad (3)$$

where E^* is the equivalent Young's modulus, and R^* is the effective radius. The definitions for E^* and R^* are respectively as follows:

$$\frac{1}{E^*} = \frac{1 - \nu_i^2}{E_i} + \frac{1 - \nu_j^2}{E_j}, \quad (4)$$

$$\frac{1}{R^*} = \frac{1}{R_i} + \frac{1}{R_j}, \quad (5)$$

where E is the Young's modulus, R is the radius, and ν is the Poisson's ratio of the two contacting sphere elements of i and j . It is noteworthy that the setting of the normal stiffness (K_n) varies widely among the analysis groups irrespective of the device type, ranging from the order of 1×10^3 N/m to 1×10^7 N/m. Although there is a large order of magnitude difference in the normal stiffness, most of the simulation results fell within the 97.5% quantile in the AOR comparison, regardless of the device type. This result suggests that the difference in the normal stiffness may not be so critical to the AOR. As the normal stiffness relates the time step of the DEM simulation in conjunction with the mass/density of the particle, we also need to check the time step used in each simulation run.

Figure 13 shows the relationships between the AOR and the normalized time step for both Device I and Device II. The normalized time step (horizontal axis) is a dimensionless quantity defined by $\frac{\Delta t}{\Delta t_{cr}}$, where Δt is the time step used in the DEM simulation and Δt_{cr} is a critical time step characterized by the particle mass M and the normal stiffness K_n ($\Delta t_{cr} = \sqrt{\frac{M}{K_n}}$). Note that the Δt settings used by each analyst were set in the range of 10^{-6} (s) to 10^{-4} (s). Most of the DEM simulations were performed with lower values of the time step than the critical time step, whereas analysis groups 1 and 2 used a large time step that exceeded the critical time step. Almost all the analysis groups set Δt within the range of 0.01 to 1.0 times of Δt_{cr} . This suggests that their aim was to improve computational efficiency by setting as large a time step as possible while ensuring stable simulation.

3.5. Summary for friction angle at contact point

Figure 14 shows the relationship between the results of the AOR experiment (on the vertical axis) and the setting

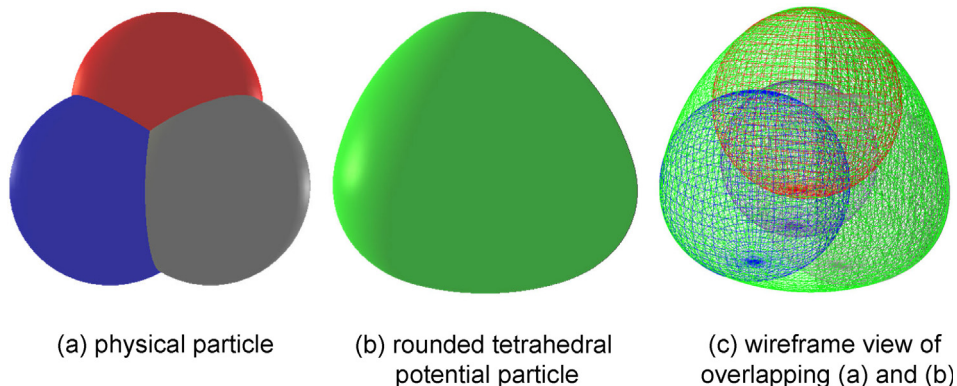


Fig. 10. Rounded tetrahedral potential particle shape modeled by analyst 6.

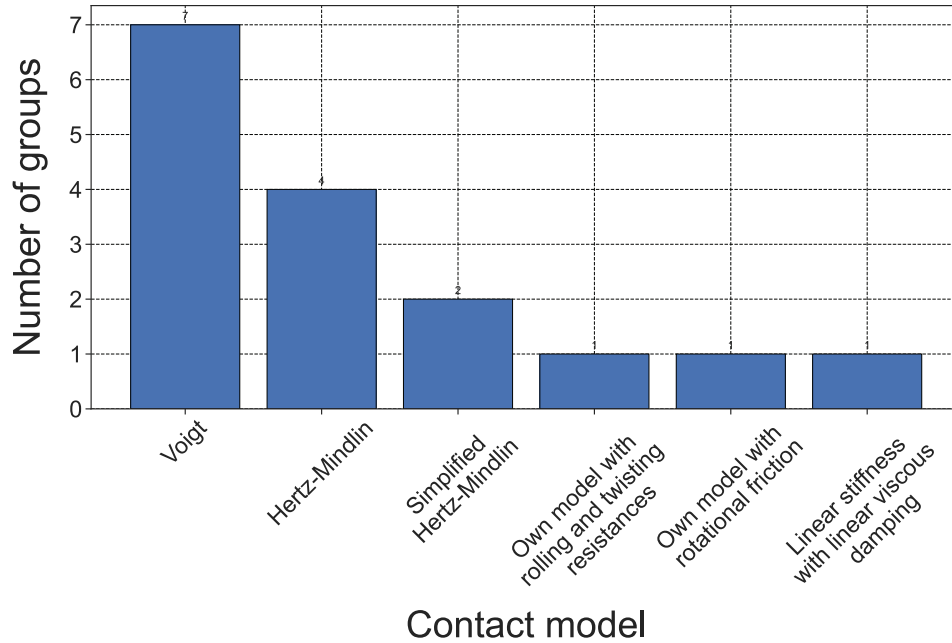


Fig. 11. Histogram of interparticle constitutive model.

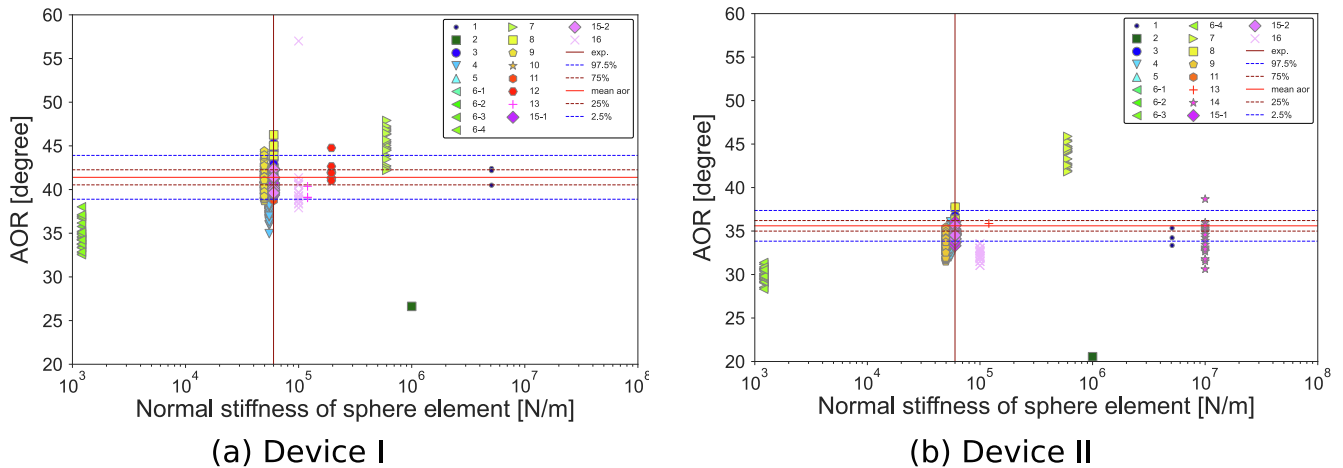


Fig. 12. Relationships between AOR experiment results and normal stiffness used in DEM simulations.

of the friction angle at the contact point configured by each analysis group (on the horizontal axis). For both devices, most of the analysis groups used the interparticle friction coefficient corresponding to the mean value of the experiment given as prior information, as listed in Table 1 ($\tan 35.5^\circ = 0.71$). One of the analysis group set the interparticle friction coefficient close to 0.5, which may be assumed to be the friction angle between the acrylic plate and the resin ($\tan 27.2^\circ = 0.51$) rather than the experimental value of the interparticle friction angle. The intermediate value close to 0.55 corresponds to the mean value of the dynamic friction coefficient obtained from the experiment ($\tan 29.36^\circ = 0.56$). It should be noted that while we can find various values for the interparticle friction angle, all of them have a certain level of accuracy in terms of correspondence with the experimental results. For exam-

ple, the use of a friction angle of 0.51 for the interparticle friction angle resulted in no significant discrepancy with the experimental results irrespective of the device type. This fact suggests that a certain level of particle shape modeling, correct particle physical properties, and appropriate boundary conditions result in good predictions of AOR. The initial configuration of the artificial particles differs from each group, but given the small variation in the results, we believe that the effect of the initial configuration is small in this round robin test.

3.6. Comparison with variability between DEM simulations and experiments

We compare the results obtained from both the DEM simulations and the experiments considering the mean

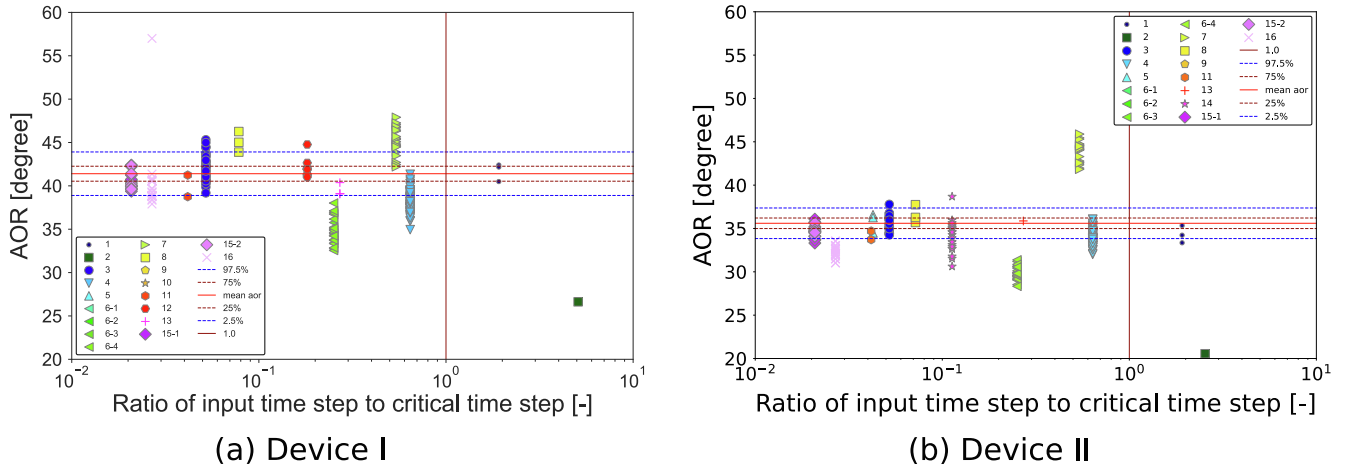


Fig. 13. Relationship between AOR experiment results and the normalized time step using the critical time step.

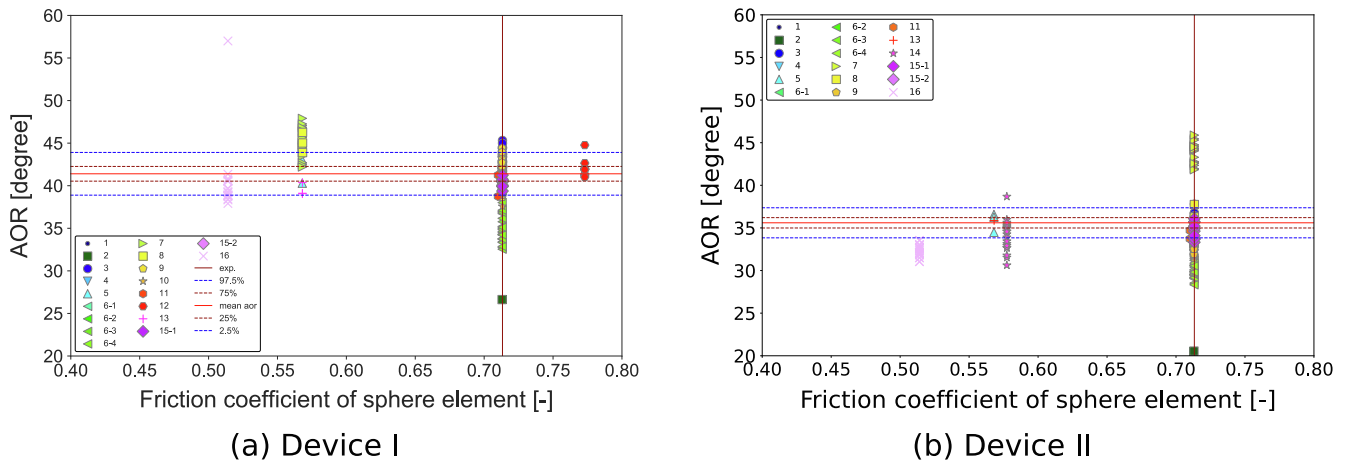


Fig. 14. Relationships between AOR experiment results and the friction angle at the contact point used in DEM simulations.

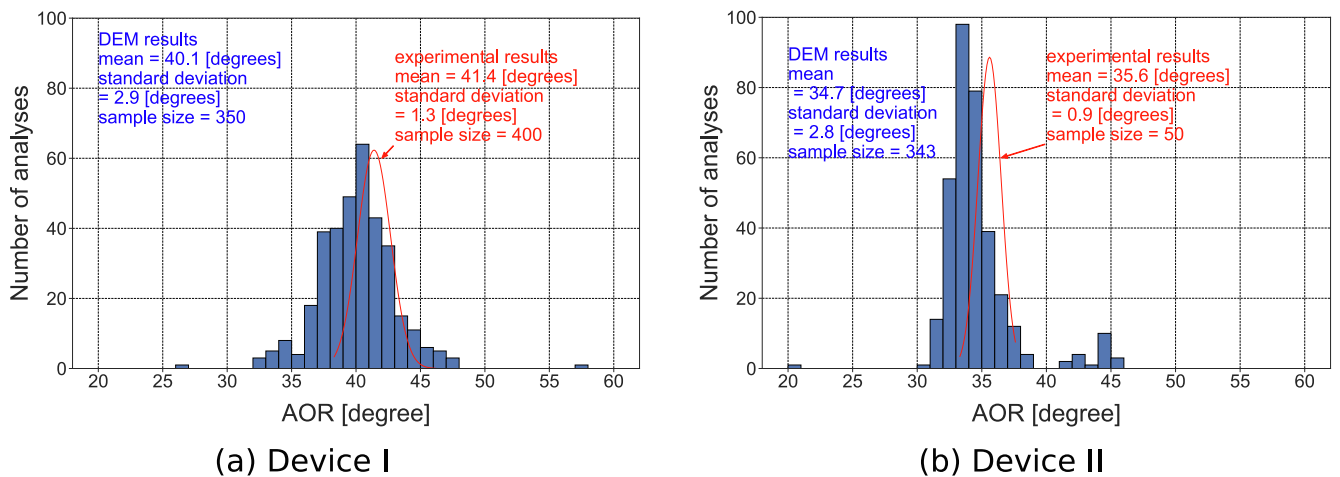


Fig. 15. Histogram of AOR based on all simulation results.

and the variations of the AOR. Note that this comparison is possible because we imposed a certain number of trials on both the experiments and DEM simulations. Figure 15 indicates the histograms of AOR (bar plot) using all DEM

simulation results for both Device I and Device II. As for Device I (Fig. 15(a)), the mean and standard deviation of the histogram (350 samples) are 40.1 degrees and 2.9 degrees, respectively, from a normal distribution approxi-

mating the histogram. Also, the red solid line shows a normal distribution with a mean of 41.4 degrees and a standard deviation of 1.3 degrees obtained from the experimental results (400 samples). Although the histogram shows a few outliers around 26 degrees and 57 degrees, it can be seen that the DEM results simulate the experimental results with considerable accuracy. In particular, the difference between the mean values is 1.3 degrees, indicating that the predictions are remarkably accurate. The variance of the DEM simulations is larger than the experimental results, but this can be attributed to the normal distribution, including the outliers.

Likewise, the DEM results for Device II have a mean value of 34.7 degrees and a standard deviation of 2.8 degrees, and the corresponding experimental values are 35.6 degrees and 0.9 degrees, respectively (Fig. 15(b)). The histogram has a bimodal shape with a small peak around 45 degrees, but the reasons for calculating an AOR greater than 40 degrees are largely due to the usage of the interparticle constitutive model with an excessive setting for rotational resistance.

4. Discussion

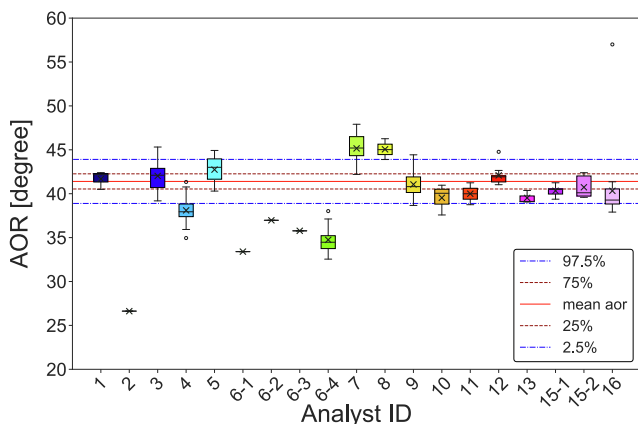
The DEM simulation results submitted by 16 groups from 7 countries were classified and statistically analyzed, and most of the simulation results were in good agreement with the experimental results. In this section, we consider the reason for the outliers from the perspective of the parameter settings. After identifying the causes of outliers, we discuss trends in DEM software.

Fig. 16 shows a side-by-side comparison of the DEM simulation results for each analysis group (16 groups in total), and the variation of each set of DEM simulation results is also represented using a box plot. The horizontal axis indicates the participating group (analysis group) ID and the vertical axis is the AOR value. The meanings of the solid and dotted lines are the same as those depicted in Fig. 9. Note that the conventions of the box plot can

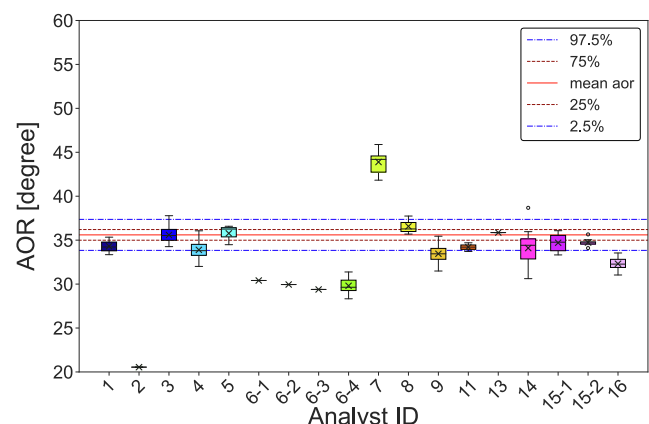
be found in Appendix A: they consist of the 25th percentile, the 50th percentile, the 75th percentile, and outliers.

In the case of Device I (Fig. 16(a)), it can be seen that the mean AOR values submitted by the five analysis groups (ID: 2, 4, 6, 7, 8) are located outside the 97.5 percentile. In the five cases with outlier results, we can identify clear reasons for such outlier results in terms of parameter settings, using convex particle shapes and usage of the interparticle constitutive equations. The time step used by analysis group 2 is significantly large, as shown in Fig. 13. Due to the use of such a large time step, it can be inferred that a large penetration occurs at the contact point, thereby resulting in a small value of the AOR. The particle density used by analysis group 4 is markedly large (10,000 kg/m³), as shown in Fig. 9. Due to the use of large density, it can be inferred that a large penetration occurs at the contact point, thereby resulting in a small value of the AOR. The convex, rounded shape of the potential particle used by analysis group 6, illustrated in Fig. 10, is likely the reason for the small value of AOR, as convex particles interlock less than the real, concave ones. Both analysis groups 7 and 8 used the interparticle constitutive model with rotation stiffness while they employed tetrahedral particles like those used in the experiment. This result in excessive moment transfer, which leads to a relatively high AOR. It should be noted that the number of simulation runs for analysis groups 2 and 4 is only one, respectively. It is possible that the mean AOR value of the simulation may approach the experimental one with a larger number of simulations.

In the case of Device II (Fig. 16(b)), it can be seen that the mean AOR values submitted by the four analysis groups (ID: 2, 6, 7, 16) are located outside the 97.5 percentile. For analysis groups 2 and 7, the reason is likely the same as that explained for Device I: parameter setting. For analysis group 6, the reason is also likely the same as that explained for Device I: particle shape (Fig. 10). However, we could not find the reason for the outlier results of



(a) Device I



(b) Device II

Fig. 16. Box plot of AOR simulation results for each participant.

analysis group 16. They used the same interparticle constitutive model with the parameter set that were used in Device I.

From the comparison between the DEM simulations and the experimental results, it was confirmed that most of the analysis groups calculated AOR values which were comparable to the experimental results irrespective of the choice of the interparticle constitutive model. There were three trends in the interparticle constitutive model: the Voigt model, the Hertz-Mindlin model and the model with rotational resistance. Most parameters of the first two models provided as prior information listed in Table 1, meanwhile no information is available for the models incorporating rotational resistance.

It should be noted that the difference in the angle of repose between these models could not be clearly distinguished. Although there were large differences in the normal stiffness individually, most analysis groups used appropriate time steps that stabilized the calculations irrespective of the magnitude of the normal stiffness and particle density. Normal stiffness is often empirically set to a value different from the measured value, which may lead to confusion for beginners. The treatise on DEM (O'Sullivan, 2011) notes that the contact between DEM particles is idealized, and it is difficult to determine the linear stiffness directly from the stiffness of the actual material. The treatise also argues that linear stiffness should conceptually be considered as a kind of "penalty spring". While the significant difference in normal stiffness was fortunately not a problem for the prediction of the angle of repose, the exact normal stiffness should be used for a task like accurately predicting the elastic wave velocity.

As confirmed by our round robin tests, the parameter settings in DEM simulations are empirical, especially in normal stiffness. It is therefore useful to establish an expert system or a flowchart for parameter setting in the DEM simulations. Interestingly, most of the analysis groups did not consider the standard deviation of each physical property shown in Table 1 when setting those parameters even though there are certain deviations in the AOR values from the DEM simulations. This implies that the variation in the particle configuration had a greater effect on the angle of repose than the variation in the physical properties.

This round robin test allowed us to consider the trend in DEM software. We found that the use of PFC3D or in-house software is relatively frequent. Moreover, we found that powerful open source DEM software was also used (Yade, LIGGGHTS, LAMMPS, Kratos). When introducing DEM software, ease of installation, documentation, richness of functions, and ease of use are important considerations, and it was determined that the open source software listed here meets these criteria. In addition to the popularization of powerful DEM software, developing software specializing in particle shape modeling (e.g., Angelidakis et al. (2021)) further promotes the use of DEM in various engineering fields.

Through these round robin tests for the angle of repose, it is reconfirmed that the parameter settings of the interparticle constitutive model and the settings of time increments are extremely important. To increase the reliability of DEM analysis, it is necessary to steadily accumulate knowledge on parameter settings. We believe that these activities will lead to the establishment of verification and validation (V&V) guidelines for DEM simulations. Finally, we touch on the prospects for future round robin tests in terms of the problem settings. There are requests to conduct triaxial compression tests with a certain level of confining pressure, but the problem settings should be decided carefully, considering the difficulty of the experiment and the abilities of many software packages to be used in the round robin test.

5. Conclusions

According to the tabulation of the DEM simulation results for two types of experimental settings, most simulation cases submitted by participants agreed with the experimental results with a certain level of accuracy in both average and variance values for the angle of repose, irrespective of the types of experiment. For a few cases where the discrepancy with the experimental results was large, it was concluded that this discrepancy was attributed to the selected values of modeling parameters, and to the employed modeling approach (i.e. clumps versus rounded convex particles). In other words, most of the software used in the round robin test works correctly providing the proper parameter settings are used. The collected data also revealed trends in the selection of the interparticle constitutive model (Voigt and Hertz-Mindlin models) and the DEM software (PFC3D, in-house, and Yade).

In future work, we will continue to conduct worldwide DEM round robin tests under the handling of the TC105 Japanese domestic committee to ensure the accuracy of the DEM simulations and the reliability of each type of DEM software.

Acknowledgement

We would like to thank Professor Catherine O'Sullivan of the Imperial College London for providing us with materials on an example for DEM verification. We also would like to express our appreciation to the participants for their cooperation: Assoc. Prof. Mitsuteru Asai of Kyushu University; Dr. Stéphane Bonelli of INRAE Aix Marseille University; Mr. Yu Hirano of the University of Tokyo; Mr. Ryoh Kuramoto of Kozo Keikaku Engineering Inc.; Prof. Takashi Matsushima of University of Tsukuba; Dr. Shintaro Ohno of Kajima corporation; Dr. Pierre Philippe of INRAE Aix Marseille University; Prof. Stefano Utili of Newcastle University; Dr. Mori Utsuno of Kajima corporation; Dr. Yishu Wang of Hohai University.

In addition, we appreciate the TC105 international committee for supporting the international activity, especially for advisement of the core members on the advertisement and invitation of the participants. Finally, we thank to the TC105 Japanese domestic committee members for their active discussion on the design of the experiments and simulations in the round robin test.

Appendix A. Box plot notation

Figure A.1 shows the details of the box plot notation used in Fig. 16. In general, the median differs from the mean and is less sensitive to outliers. Hence, the median is useful when the data does not obey the normal distribution.

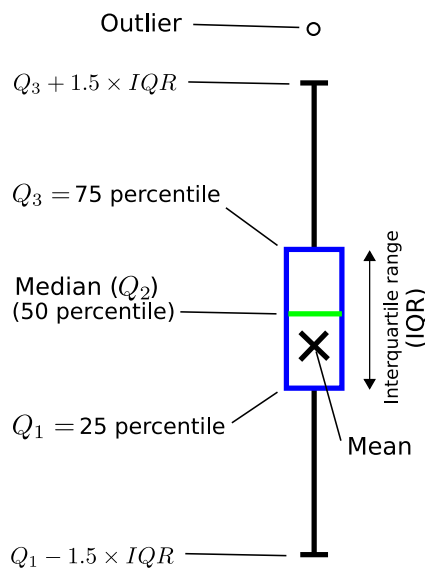


Fig. A.1. Box plot notation.

References

- Angelidakis, V., Nadimi, S., Utili, S., 2021. SHape analyser for particle engineering (SHAPE): Seamless characterisation and simplification of particle morphology from imaging data. *Comput. Phys. Commun.* 265, 107983.
- Berre, I., Boon, W.M., Flemisch, B., Fumagalli, A., Gläser, D., Keilegavlen, E., Scotti, A., Stefansson, I., Tatomir, A., Brenner, K., Burbulla, S., Devloo, P., Duran, O., Favino, M., Hennicker, J., Lee, I. H., Lipnikov, K., Masson, R., Mosthaf, K., Nestola, M.G.C., Ni, C. F., Nikitin, K., Schädle, P., Svyatskiy, D., Yanbarisov, R., Zulian, P., 2021. Verification benchmarks for single-phase flow in three-dimensional fractured porous media. *Adv. Water Resour.* 147, 103759.
- Chen, J., Furuichi, M., Nishiura, D., 2020. Discrete element simulation and validation of a mixing process of granular materials. *Materials*, 13.
- Chen, J., Kitamura, A., Barbieri, E., Nishiura, D., Furuichi, M., 2022. Analyzing effects of microscopic material parameters on macroscopic mechanical responses in underwater mixing using discrete element method. *Powder Technol.* 401, 117304.
- Cheng, Y.P., Nakata, Y., Bolton, M.D., 2003. Discrete element simulation of crushable soil. *Géotechnique* 53, 633–641.
- Chew, K., Chiaro, G., Vinod, J.S., A., T., Allulakshmi, K., 2022. Direct shear behavior of gravel-rubber mixtures: discrete element modeling and microscopic investigations. *Soils Found.* (in press).
- Cundall, P.A., 1971. A computer model for simulating progressive, large-scale movement in blocky rock system. In: *Proceedings of the International Symposium on Rock*, Nancy, France 2, pp. 129–136.
- Cundall, P.A., Strack, O.D.L., 1979. A discrete numerical model for granular assemblies. *Géotechnique* 29, 47–65.
- Dadvand, P., Rossi, R., Gil, M., Martorell, X., Cotela, J., Juanpere, E., Idelsohn, S.R., Oñate, E., 2013. Migration of a generic multi-physics framework to HPC environments. *Comput. Fluids* 80, 301–309.
- Dadvand, P., Rossi, R., Oñate, E., 2010. An object-oriented environment for developing finite element codes for multi-disciplinary applications. *Arch. Comput. Methods Eng.* 17, 253–297.
- Duriez, J., Darve, F., Donzé, F.V., 2011. A discrete modeling-based constitutive relation for infilled rock joints. *Int. J. Rock Mech. Min. Sci.* 48, 458–468.
- Furuichi, M., Nishiura, D., Asai, M., Hori, T., 2017. The first real-scale DEM simulation of a sand-box experiment using 2.4 billion particles. *The International Conference for High Performance Computing, Networking, Storage and Analysis* URL: https://sc17.supercomputing.org/SC17%20Archive/tech_poster/tech_poster_pages/post113.html.
- Harris, R.A., Barall, M., Aagaard, B., Ma, S., Roten, D., Olsen, K., Duan, B., Liu, D., Luo, B., Bai, K., Ampuero, J., Kaneko, Y., Gabriel, A., Duru, K., Ulrich, T., Wollherr, S., Shi, Z., Dunham, E., Bydlon, S., Zhang, Z., Chen, X., Somala, S.N., Pelties, C., Tago, J., Cruz-Atienza, V.M., Kozdon, J., Daub, E., Aslam, K., Kase, Y., Withers, K., Dalguer, L., 2018. A suite of exercises for verifying dynamic earthquake rupture codes. *Seismol. Res. Lett.* 89, 1146–1162.
- Harris, R.A., Barall, M., Andrews, D.J., Duan, B., Ma, S., Dunham, E. M., A. Gabriel, A., Kaneko, Y., Kase, Y., Aagaard, B.T., Oglesby, D. D., P. Ampuero, J., Hanks, T.C., Abrahamson, N., 2011. Verifying a computational method for predicting extreme ground motion. *Seismol. Res. Lett.* 82, 638–644.
- Horrillo, J., Grilli, S.T., Nicolisky, D., Roeber, V., Zhang, J., 2015. Performance benchmarking tsunami models for NTHMP's inundation mapping activities. *Pure Appl. Geophys.* 172, 869–884.
- Irazábal, J., Salazar, F., Oñate, E., 2017. Numerical modelling of granular materials with spherical discrete particles and the bounded rolling friction model. application to railway ballast. *Comput. Geotech.* 85, 220–229.
- Itasca Consulting Group, Inc., 2021. PFC — Particle Flow Code, Minneapolis: Itasca.
- Jiang, M., Liu, A., Wang, H., Lu, G., Li, L., 2020. An empirical strength criterion for deep rock incorporating the effect of fracture intensity using distinct element method. *IOP Conf. Ser.: Earth Environ. Sci.* 570, 022060.
- Jiang, M., Shen, Z., Wang, J., 2015. A novel three-dimensional contact model for granulates incorporating rolling and twisting resistances. *Comput. Geotech.* 65, 147–163.
- Kanno, H., Moriguchi, S., Hayashi, S., Terada, K., 2021. A computational design optimization method for rockfall protection embankments. *Eng. Geol.* 284, 105920.
- Kikkawa, N., Hori, T., Itoh, K., Mitachi, T., 2013. Study on a determination manner of discrete element method parameters in a bonded granular material. *Japanese Geotech. J.* 8, 221–237 (in Japanese).
- Kloss, C., Goniva, C., Hager, A., Amberger, S., Pirker, S., 2012. Models, algorithms and validation for opensource DEM and CFD-DEM. *Progress Comput. Fluid Dyn. Int. J.* 12, 140–152.
- Kono, A., 2018. Validation of numerical simulation using 3d-discrete element ballasted track model. In: *Computers in Railways XVI: Railway Engineering Design and Operation*, WIT Press, Southampton UK, pp. 169–177.
- Lin, Z.Y., Wang, Y.S., Tang, C.S., Cheng, Q., Zeng, H., Liu, C., Shi, B., 2021. Discrete element modelling of desiccation cracking in thin clay layer under different basal boundary conditions. *Comput. Geotech.* 130, 103931.
- Matsushima, T., Saomoto, H., 2002. Discrete element modeling for irregularly-shaped sand grains. In: *NUMGE 2002. 5th European Conference Numerical Methods in Geotechnical Engineering*, pp. 239–246.

- Nakase, H., Iwamoto, T., Cao, G., Tabei, K., Sakaguchi, H., Matsushima, T., 2017. Reproduction analysis of actual slope collapse and parametric study for evacuation of the deposit volume by a simple model of distinct element method. *J. Japan Soc. Civil Eng., Ser. A1 (Structural Engineering & Earthquake Engineering (SE/EE)) (in Japanese)* 73, I_694–I_703.
- Nakata, Y., Moriguchi, S., Kajiyama, S., Kido, R., Kikkawa, N., Saomoto, H., Takano, D., Higo, Y., 2022. Experimental data of 3D printed granular material for verification of discrete element modelling simulation. *Soils Found.* (in press)
- Nishiura, D., Furuichi, M., Sakaguchi, H., 2021. Real-scale DEM simulations on the fault evolution process observed in sandbox experiments. *Adv. Powder Technol.* 32, 4432–4441.
- Nishiura, D., Sakai, H., Aikawa, A., Tsuzuki, S., Sakaguchi, H., 2018. Novel discrete element modeling coupled with finite element method for investigating ballasted railway track dynamics. *Comput. Geotech.* 96, 40–54.
- O'Sullivan, C., 2011. *Particulate Discrete Element Modelling: A Geomechanics Perspective*. CRC Press.
- Otsubo, M., O'Sullivan, C., 2018. Experimental and DEM assessment of the stress-dependency of surface roughness effects on shear modulus. *Soils Found.* 58, 602–614.
- Otsubo, M., O'Sullivan, C., Hanley, K.J., Sim, W.W., 2017. The influence of particle surface roughness on elastic stiffness and dynamic response. *Géotechnique* 67, 452–459.
- Sakaguchi, H., Nishiura, D., 2009. Development of hyper intelligent discrete element method (HiDEM) and its application for science and industry. *JAMSTEC Report of Res. Develop.* 2009, 201–209 (in Japanese).
- Sandia National Laboratories, 2001. LAMMPS molecular dynamics simulator. URL: <https://www.lammps.org/index.html>. Accessed: 2021-11-4.
- Shimizu, H., Murata, S., Ishida, T., 2011. The distinct element analysis for hydraulic fracturing in hard rock considering fluid viscosity and particle size distribution. *Int. J. Rock Mech. Min. Sci.* 48, 712–727.
- Smilauer, V., Angelidakis, V., Catalano, E., Caulk, R., Chareyre, B., Chèvremont, W., Dorofeenko, S., Duriez, J., Dyck, N., Elias, J., Er, B., Eulitz, A., Gladky, A., Guo, N., Jakob, C., Kneib, F., Kozicki, J., Marzougui, D., Maurin, R., Modenese, C., Pekmezi, G., Scholtés, L., Sibille, L., Stransky, J., Sweijen, T., Thoeni, K., Yuan, C., 2021. Yade documentation. The Yade Project. URL: <https://doi.org/10.5281/zenodo.5705394>.
- TC105 Japanese domestic committee, 2020. Round robin test of angle of repose (AOR). URL: <http://geotech.civil.yamaguchi-u.ac.jp/tc105/>. Accessed: 2021-9-21.
- Thompson, A.P., Aktulga, H.M., Berger, R., Bolintineanu, D.S., Brown, W.M., Crozier, P.S., in 't Veld, P.J., Kohlmeyer, A., Moore, S.G., Nguyen, T.D., Shan, R., Stevens, M.J., Tranchida, J., Trott, C., Plimpton, S.J., 2022. LAMMPS - a flexible simulation tool for particle-based materials modeling at the atomic, meso, and continuum scales. *Comput. Phys. Commun.* 271, 108171.
- Tsuji, K., Asai, M., Konishi, Y., Oomine, S., 2019. Sph-Dem coupling simulation with a liquid bridge force for the representation of ground collapse phenomenon. *J. Japan Soc. Civil Eng., Ser. A2 (Applied Mechanics (AM)) (in Japanese)* 75, I_203–I_213.
- Yamaguchi, A., Maeda, K., Matsuda, T., Takagi, K., 2017. Fluidity and pore water pressure variation in the sandy ground induced by surface layer flow using dem-cfd. *J. Japan Soci. Civil Eng. Ser B2 (Coastal Engineering) (in Japanese)* 73, I_517–I_522.
- Yu, Y., Cheng, Y.P., Xu, X., Soga, K., 2016. Discrete element modelling of methane hydrate soil sediments using elongated soil particles. *Comput. Geotech.* 80, 397–409.
- Zeghal, M., El Shamy, U., 2004. A continuum-discrete hydromechanical analysis of granular deposit liquefaction. *Int. J. Numer. Anal. Meth. Geomech.* 28, 1361.